NEWS-G: Light dark matter search with a Spherical Proportional Counter

Konstantinos Nikolopoulos[*]

University of Birmingham
Birmingham, B15 2TT
United Kingdom
E-mail: k.nikolopoulos@bham.ac.uk

The New Experiments With Spheres-Gas (NEWS-G) Collaboration aims to shed light on the dark matter sector using the Spherical Proportional Counter. NEWS-G uses light noble gases as targets, to search for light dark matter in the 0.1 – 10 GeV range. SEDINE, a 60 cm in diameter spherical proportional counter, already operates in the Underground Laboratory of Modane, while the full-scale detector – 140 cm in diameter – is currently under construction. The first results from NEWS-G, based on 9.7 kg·days of exposure, are presented, obtaining a 90% confidence level upper limit of $4.4 \cdot 10^{37}$ cm^2 on the nucleon-dark matter interaction cross-section for a candidate with a mass 0.5 GeV. Recent developments in various aspects of the detector are discussed, along with the status of the project and future prospects.

---

[*]Speaker.

1. Introduction

It is established from a variety of astrophysical observations [1, 2] and precise measurements of the Cosmological Microwave Background [3] that approximately 84.5% of the matter content of our Universe consists of non-baryonic cold Dark Matter (DM). Although the nature of DM is currently unknown, many theories beyond the Standard Model (SM) predict massive neutral particles, thermally produced in the early Universe, that could account for the observed DM relic density: a generic class of well motivated DM candidates known as Weakly Interacting Massive Particles (WIMPs) [4]. The WIMP hypothesis favours DM masses in the 10 – 1000 GeV range [5]. However, given the lack of evidence for supersymmetry at the LHC [6] and of convincing evidence from direct and indirect detection experiments motivates a broader approach to the DM question, including the investigation of models that would lead to lighter DM candidates with potentially more complex couplings: hidden sectors [7, 8], asymmetric dark matter [9, 10], but also more generic descriptions through effective theory [11].

Direct detection experiments aim to detect incoming DM particles from the Milky Way halo via their coherent elastic scattering off a target nuclei. The expected event rates are orders of magnitude lower than natural radioactivity, requiring large exposures with detectors made of radiopure materials, shielded and operated deep underground to protect against ambient radioactivity and cosmic rays, respectively. Additional experimental challenges arise from the shape of the expected nuclear recoil energy spectrum,

Figure 1: DM-nucleon interaction cross sections per nucleon for spin-independent coupling versus mass, from Ref. [12].

concentrated to ever lower energies as the candidate mass, m_χ, decreases, making low energy detection thresholds critical for sensitivity to low mass candidates. Moreover, the ionization quenching factor – the fraction of energy released by a recoil in a medium through ionization compared to its total kinetic energy – depends on the nucleus atomic number and kinetic energy. At low kinetic energies, of a few keV, the ionization produced in a medium decreases as the energy decreases.

Current experimental constraints are summarised in Fig. 1. The upper limits set on the spin-independent DM-nucleon scattering cross section, σ_{SI}, in the low mass range are orders of magnitude weaker than those at higher masses [13, 14], purely due to the detection energy threshold requirements. Thus, a wide region of the parameter space (σ_{SI}, m_χ) can be probed with low energy detection thresholds without relying on tonne-scale absorbers.

2. The Spherical Proportional Counter

The NEWS-G collaboration, consisting of 10 institutes from 5 countries, aims to search for DM candidates in the 0.1 – 10 GeV range. The experiment exploits the novel technology of Spherical Proportional Counters [15, 16, 17]. The detector, presented in Fig. 3, consists of a grounded spherical shell which acts as the cathode and a small spherical anode, the sensor, supported at the
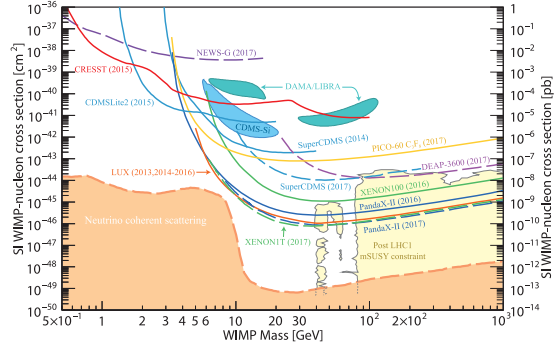
centre by a grounded metallic rod, to which the high voltage is applied and from which the signal is read-out. In the ideal case the electric field has an $1/r^2$ dependence on the radial distance from the detector centre. This dependence naturally divides the detector into the drift region, where under the influence of the low electric field the electrons drift towards the anode, and the amplification region, where charge multiplication occurs.

The spherical geometry provides several advantages compared to other detector geometries, such as parallel plates or cylinders, for building large volume detectors. The sphere has the lowest surface to volume ratio and it is the most suited for high pressure operation. In addition, it has the lowest capacitance, which is approximately proportional to the anode radius and independent of the radius of the metallic shell. Overall, the spherical proportional counter exhibits the following key features: a) very low energy thresholds, down to single ionization electron detection, thanks to low sensor capacitance independently of the detector volume and high gain operation; b) small number of readout channels and potential for directionality; c) background rejection and fiducialisation through pulse shape analysis; d) simplicity, robustness, and use of highly radiopure materials; e) variety of light target gases, allowing optimisation of momentum transfers for low-mass particles in the GeV mass range, significantly increasing the sensitivity to sub-GeV candidates; and f) possibility to vary the operational pressure and high voltage, providing additional handles to disentangle potential signals from unknown backgrounds.
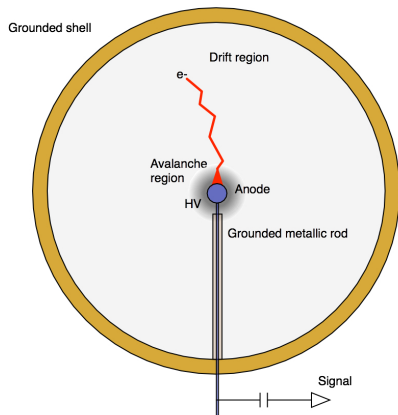
3. First NEWS-G result on search for light DM

Figure 2: Spherical proportional counter design and principle of operation [17].

The ⌀60 cm spherical proportional counter SEDINE already operates at the Laboratoire Souterrain de Modane (LSM) inside the Frejus tunnel. This is one of the deepest laboratories in the world, with an overburden of 4800 m water equivalent. The detector, shown in Fig. 3(a), is constructed using ultra pure (NOSV) copper, which was chemically cleaned for removal of Radon deposits, and a ⌀6.3 mm spherical sensor made of silicon, shown in Fig. 3(b). Additional shielding layers protect SEDINE from external radiation, as shown in Fig. 3(c). The gas mixture used for these first results is Ne/CH$_4$ (99.3%/0.7%) at a pressure of 3.1 bar. This gives a total target mass of 282 g. The sensor high voltage was 2520 V and it was read-out with a CANBERRA Model 2006 charge sensitive preamplifier. The detector was operated continuously, in sealed mode, for 42.7 days.

For detector calibration ^{37}Ar and ^{241}Am-^{9}Be sources were used. The ^{37}Ar gas was inserted to the detector at the end of the run, providing mono-energetic events at 2.82 keV and 270 eV from X-rays induced by electron capture in the K- and L-shells, respectively. The ^{241}Am-^{9}Be neutron source was used to induce nuclear recoil events, homogeneously distributed in the detector volume, down to low energy range relevant for sub-GeV DM candidates.

(a)   (b)   (c)

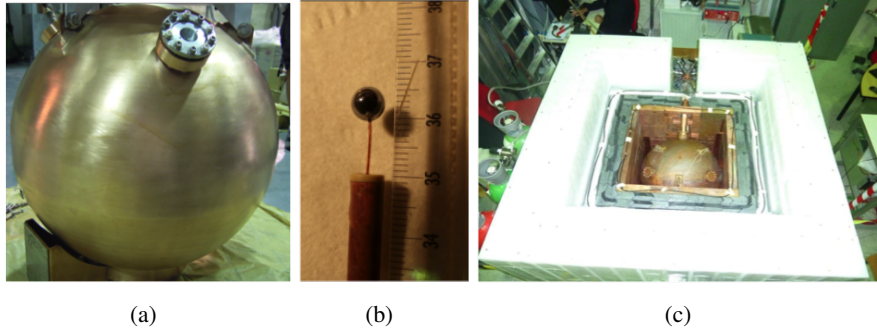**Figure 3:** (a) SEDINE, the ⌀60 cm spherical proportional counter operating at LSM; (b) the sensor installed in SEDINE with a ⌀6.3 mm silicon spherical anode and a ⌀380 μm diameter insulated HV wire routed through a grounded copper rod; and (c) the cubic shielding of SEDINE, moving outwards, comprises 8 cm of copper, 15 cm of lead, and 30 cm of polyethylene.
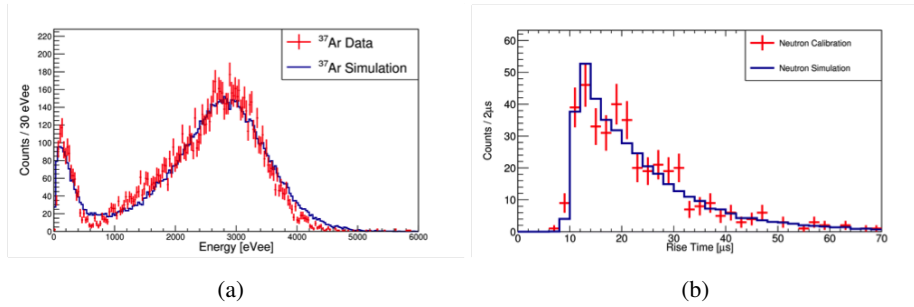

(a)   (b)

Figure 4: (a) Energy distribution of the ^{37}Ar calibration data, clearly exhibiting the 2.82 keV and 270 eV peaks (red markers). The overlaid simulation (dark blue histogram) shows good agreement [18]. (b) Rise time distribution of ^{241}Am-^{9}Be calibration events in the energy range 150 – 250 eVee (red markers). The overlaid simulation (dark blue histogram) shows good agreement [18].

4. Detector simulation and background modeling

The response of the detector to ionising radiations was simulated, accounting for the processes that take place during detector operation: a) the primary ionization for electronic and nuclear recoils, including a SRIM-derived [19] ionisation quenching factor for the latter; b) the electric field for as-installed detector geometry, calculated using finite element method software; c) the drift and diffusion of primary charges as parametrized by Magboltz [20]; and d) the avalanche process, simulated by Garfield++ [21] and accounting for Penning transfers [22]. The output pulse for a given event was the sum of the contributions from all the ionisation electrons that reached the anode. To these pulses, a baseline, including noise randomly chosen from empty events recorded during the physics-run, was added. The simulated data were subsequently processed and analysed with the same algorithms and software as the recorded data.

The simulation was validated using calibration data. In Fig. 4(a) the simulation results are compared to ^{37}Ar data and good agreement is observed, including non-trivial effects such as the reproduction of the non-Gaussianity of the 2.82 keV line caused by the field anisotropy in the avalanche region. In Fig. 4(b) the respective comparison with the ^{241}Am-^{9}Be data is presented, demonstrating good agreement in the rise time distribution of the neutron induced nuclear recoils.

The background contributions in this search are categorised into surface and volume events. Surface events are uniformly distributed in the inner surface of the vessel and originate predominantly from radon daughter decays. Volume events originate from high energy γ-rays from ^{208}Tl and ^{40}K present in the rock from the decay chains of ^{238}U and ^{232}Th contained in the copper shell, and the detector shielding. It has been demonstrated through simulations that the pulse rise time provides useful statistical discrimination against surface events down to the analysis threshold.

5. Data analysis and results

An analysis energy threshold of 150 eVee was used, substantially above the trigger threshold of approximately 36 eVee, to ensure practically 100% trigger efficiency. Furthermore, an artifical deadtime of 4 s was applied following every triggered event. This requirements removes non-physical events at the cost of a 20.1% exposure loss. Subsequently, the Region Of Interest (ROI) is defined, by requiring that the pulses have a rise time between 10 and 32 μs and an energy between 0.15 and 4 keV. The expected background was estimated using sideband regions. Specifically, the event rate in the 4 – 6 keVee energy range was used to estimate the expected Compton background, while the region with rise times above 32 μs was used to estimate the expected number of surface events. The total exposure was 9.7 kg·days and 1620 events were recorded in the ROI.

The signal regions were optimised separately for various DM signal mass hypotheses using a Boosted Decision Tree (BDT); a machine learning algorithm which was trained with 10^5 simulated background events and signal events for 8 different DM candidate masses from 0.5 to 16 GeV. For each mass point, events were classified as signal- or background-like using the BDT score. Further details can be found in Ref. [18].

For each mass, considering as candidates all the events observed in the corresponding signal region, 90% Confidence Level (CL) upper limit on the spin-independent DM-nucleon scattering cross section was derived using Poisson statistics. The recoil energy spectrum used to derive the sensitivity to light DM is based on standard assumptions of the DM-halo model[1]. The resulting exclusion limit is presented at Fig. 5 as a solid red line, setting new constraints on the spin-independent WIMP-nucleon scattering cross-section below 0.6 GeV. A cross-section of 4.4×10^{-37} cm^2 for a 0.5 GeV light DM candidate mass is excluded at 90% CL.

6. Developments in sensor design

The design of the sensor and its support structure are crucial for the performance of the detector. Substantial amount of effort is invested in this direction, aiming to produce design with better characteristics. Two main lines of development are pursued: a) single-anode sensors; and b) multi-anode sensors. Recent developments in both directions are discussed.

6.1 Single-anode sensors

The inclusion of a correction electrode, which in the design described above is just the grounded rod, is essential for the good performance of the detector as it shields the volume of the detec-

---

[1]DM density $\rho_{DM} = 0.3$ GeV/cm^3, galactic escape velocity $v_{esc} = 544$ km/s, asymptotic circular velocity $v_0 = 220$ km/s
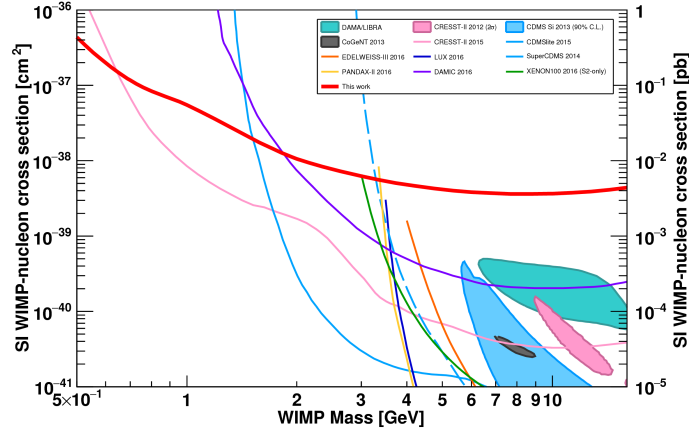
Figure 5: Constraints in the spin-independent WIMP-nucleon cross section versus WIMP mass plane. The result from this analysis is shown in solid red [18].

tor from the anode wire and improves the electric field homogeneity for zenith angles near the wire [15]. However, further improvements in the field homogeneity are required, and in this led to the development of the resistive glass electrode prototypes [23].
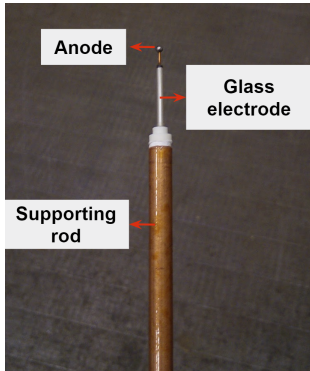

Figure 6: Module with a cylindrical glass correction electrode [23].

In Fig. 6, the constructed module is presented, composed of a 2 mm diameter anode made of stainless steel. The glass tube has a length of 20 mm and the distance between the ending edge of the tube and the surface of the anode is 3 mm. The details of the detector design are given in Ref. [23]. The module is at the centre of a spherical, stainless steel vessel of 15 cm radius and is supported by a copper rod with a 4 mm (6 mm) inner (outer) diameter. The connection interface between the rod and the detector's spherical vessel ensures that both be grounded.

The achieved electric field homogeneity was tested experimentally using an ^{55}Fe source was placed inside the detector. The location of this collimated source could be changed during detector operation. ^{55}Fe decays through electron capture to ^{55}Mn emitting 5.9 keV X rays. Data were collected with the source located at $90°$ and $180°$ to the grounded rod and the rise time of signals versus their amplitude is shown in Fig. 7(b), demonstrating similar response in both cases. Thus, electric field distortions are corrected for by the second correction electrode.

The detector operation stability was tested using He:Ar:CH$_4$ (87%:10%:3%) at 2 bar, introduced using a filter to remove oxygen and water traces. The 6.4 keV X ray fluorescence of the ^{55}Fe K-line, induced by environmental γ-rays and cosmic muons, was used to monitor the gas gain as a function of time, as shown in Fig. 7(a) for 12 days of continuous data-taking. The detector was stable throughout the entire period, with no spark-induced gain variations. The observed gradual decrease of the pulse height is due to the gradual introduction of contaminants to the detector.
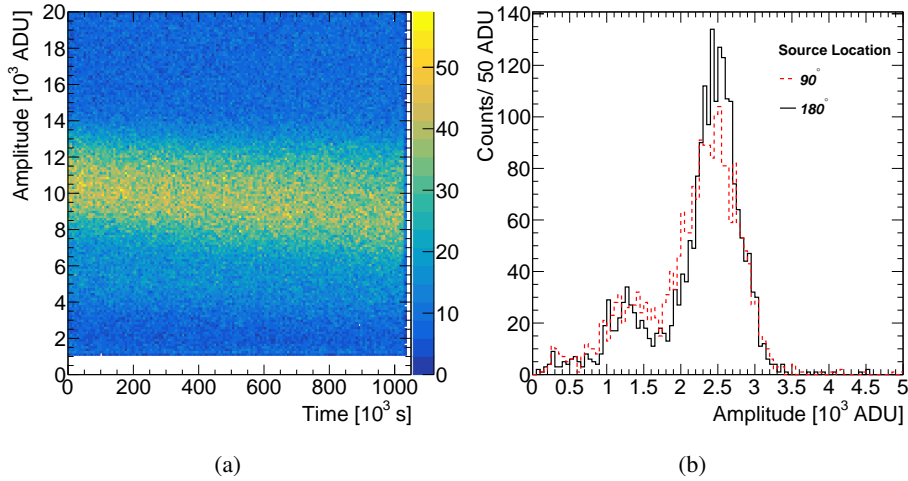
(a)	(b)

Figure 7: (a) Pulse height as a function of time using a detector filled with 2 bar of He:Ar:CH$_4$ (87%:10%:3%). The anode voltage was 2350 V, while the second correction electrode was grounded. (b) Rise time versus amplitude for recorded pulses for 5.9 keV X rays from an ^{55}Fe source located inside the detector placed at zenith angle of 90° and 180°, relative to the grounded rod. The detector is filled with He:Ar:CH$_4$ (92%:5%:3%) at 1 bar. The anode and second correction electrode voltages are set at 1450 V and 200 V, respectively. Both figures from Ref. [23]

6.2 Multi-anode sensors

One of the challenges towards development of large size spherical proportional chambers is the intimate coupling of the detector gain and the electron drift velocity, in particular at large radii, to the electric field of the single-anode. Increasing the electric field of the anode could efficiently collect the ionisation electrons at large radii, but could lead to breakdown during the avalanche creation, while an electric field providing an acceptable gas gain, could be inefficient for the effective collection of the charges.

Figure 8: ACHINOS prototype with 11 balls of ⌀2 mm constructed using 3D printing [24].

For this reason, ACHINOS [24] a new multi-ball sensor is being developed, composed of multiple anode balls equidistantly placed on a virtual spherical surface and all biased at the same potential, as shown in Fig. 8. Collectivelly, this leads to an increased electric field magnitude at large radii, while maintaining the ability to reach high gain operation provided by anode diameter in the order of a mm. For example an ACHINOS sensor with 11 balls distributed on a ⌀36 mm diameter sphere produces approximately 9 times larger electric field at large radii, with respect to a single ⌀2 mm anode placed at the same bias voltage [24]. This development paves the way for large detector operation under high pressure.

7. Towards a large size detector

The next phase of the experiment will build upon the experience acquired from the operation of SEDINE at LSM. It will consist of a sphere 140 cm in diameter, made of Aurubis (C10100) low activity copper. To further suppress background contributions from the detector material, an approximately 0.5 mm thick cladding-type layer of ultra-pure copper has been electroplated onto the inner surface. The new detector is expected to be operational during the summer of 2019. Initial commissioning will take place at LSM and, subsequently, the detector will be transfered to SNOLAB, with an overburden of 6000 m water equivalent, for the main physics run.

Beyond the improvements on the detector construction, a new, compact design for the shielding is envisioned. It will consist of a shell with 3 cm of archaeological lead and 22 cm low-activity lead, which will be placed inside a 40 cm thick polyethylene shield. The new setup will include dedicated handling to avoid radon entering the detector at any time. These improvements are expected to lead to a significant reduction of the backgrounds levels, relative to those of SEDINE, and will allow sensitivity down to cross sections of $\mathcal{O}\left(10^{-41}\ \mathrm{cm}^2\right)$. The use of hydrogen and helium-rich targets will open up the experimental reach down to DM candidate masses of 0.1 GeV.

8. Conclusions

The spherical proportional counter is a novel gaseous detector offering significant advantages in the search for light dark matter candidates in the range between 0.1 and 10 GeV. The first physics results of the NEWS-G collaboration were obtained using the SEDINE detector, a 60 cm in diameter spherical proprtotional counter, operating at LSM. These results demonstrate the potential of spherical proportional counters in the search of low-mass DM candidates. A new, 140 cm in diameter, detector is currently under construction and will be commissioned at LSM in the summer of 2019, before being transfered to SNOLAB. Several improvements, based on the experience from SEDINE, have been included in the design, including using low-activity copper, as well as electroplating a layer of ultra-pure copper onto the inner surface of the detector. Moreover, a new, compact shielding is enviosned. These improvements, together with the developments in sensor design – including new single- and multi-sensor anodes – are expected to lead to substantial improvements in the sensitivity. Future runs with hydrogen rich gas mixtures will optimise the momentum transfer for DM candidates in the GeV mass range, and will provide sensitivity to sub-GeV light DM.

References

[1] J. Silk et al., *Particle Dark Matter: Observations, Models and Searches*. Cambridge Univ. Press, Cambridge, 2010.

[2] D. Clowe et al., *A Direct Empirical Proof of the Existence of Dark Matter*, The Astrophysical Journal Letters **648** (2006) no. 2, L109.

[3] Planck Collaboration, *Planck 2015 results - XIII. Cosmological parameters*, Astronomy & Astrophysics **594** (2016) A13.

[4] J. L. Feng, *Dark Matter Candidates from Particle Physics and Methods of Detection*, Ann. Rev. Astron. Astrophys. **48** (2010) 495–545.

[5] G. Jungman, M. Kamionkowski, and K. Griest, *Supersymmetric dark matter*, Phys. Rept. **267** (1996) 195–373.

[6] O. Buchmueller et al., *The CMSSM and NUHM1 in Light of 7 TeV LHC, $B_s \to \mu^+\mu^-$ and XENON100 Data*, Eur. Phys. J. **C72** (2012) 2243.

[7] R. Essig et al., *Working Group Report: New Light Weakly Coupled Particles*, in *Proceedings, 2013 Community Summer Study on the Future of U.S. Particle Physics: Snowmass on the Mississippi*. 2013. arXiv:1311.0029 [hep-ph].

[8] S. Profumo, *GeV dark matter searches with the NEWS detector*, Phys. Rev. **D93** (2016) 055036.

[9] K. Petraki and R. R. Volkas, *Review of asymmetric dark matter*, Int. J. Mod. Phys. **A28** (2013) 1330028.

[10] K. M. Zurek, *Asymmetric Dark Matter: Theories, Signatures, and Constraints*, Phys. Rept. **537** (2014) 91–121.

[11] SuperCDMS Collaboration, *Dark matter effective field theory scattering in direct detection experiments*, Phys. Rev. **D91** (2015) 092004.

[12] Particle Data Group Collaboration, M. Tanabashi et al., *Review of Particle Physics*, Phys. Rev. **D98** (2018) no.~3, 030001.

[13] CRESST Collaboration, *Results on light dark matter particles with a low-threshold CRESST-II detector*, Eur. Phys. J. **C76** (2016) no.~1, 25.

[14] SuperCDMS Collaboration, *Search for Low-Mass Weakly Interacting Massive Particles with SuperCDMS*, Phys. Rev. Lett. **112** (2014) no.~24, 241302.

[15] I. Giomataris et al., *A Novel large-volume Spherical Detector with Proportional Amplification read-out*, JINST **3** (2008) P09007.

[16] G. Gerbier et al., *NEWS : a new spherical gas detector for very low mass WIMP detection*, arXiv:1401.7902 [astro-ph.IM].

[17] I. Savvidis et al., *Low energy recoil detection with a spherical proportional counter*, arXiv:1606.02146 [physics.ins-det].

[18] NEWS-G Collaboration, Q. Arnaud et al., *First results from the NEWS-G direct dark matter search experiment at the LSM*, Astropart. Phys. **97** (2018) 54–62, arXiv:1706.04934 [astro-ph.IM].

[19] J. Biersack and L. Haggmark, *A Monte Carlo computer program for the transport of energetic ions in amorphous targets*, Nuclear Instruments and Methods **174** (1980) no.~1, 257 – 269.

[20] S. F. Biagi, *Monte Carlo simulation of electron drift and diffusion in counting gases under the influence of electric and magnetic fields*, Nucl. Instrum. Meth. **A421** (1999) no.~1-2, 234–240.

[21] R. Veenhof, *GARFIELD, recent developments*, Nucl. Instrum. Meth. **A419** (1998) 726–730.

[22] F. M. Penning, *Über Ionisation durch metastabile Atome*, Naturwissenschaften **15** (1927) 818.

[23] I. Katsioulas, I. Giomataris, P. Knights, M. Gros, X. F. Navick, K. Nikolopoulos, and I. Savvidis, *A sparkless resistive glass correction electrode for the spherical proportional counter*, JINST **13** (2018) no.~11, P11006, arXiv:1809.03270 [physics.ins-det].

[24] A. Giganon, I. Giomataris, M. Gros, I. Katsioulas, X. F. Navick, G. Tsiledakis, I. Savvidis, A. Dastgheibi-Fard, and A. Brossard, *A multiball read-out for the spherical proportional counter*, JINST **12** (2017) no.~12, P12031, arXiv:1707.09254 [physics.ins-det].